New Materials, Compounds and Applications
Vol.9, No.2, 2025, pp.240-253
https://doi.org/10.62476/nmca.92240

0D TITANIUM DIOXIDE AND 2D CARBON NITRIDE HETEROJUNCTION FOR ENHANCED TETRACYCLINE DEGRADATION

Guo Maode[1,2], Li He[1], Rezki Ismail[2], Karimah Kassim[3], Lim Ying Chin[2*]

[1]Department of Chemistry, Hengshui University, Hengshui, China
[2]School of Chemistry and Environment, Faculty of Applied Sciences, Universiti Teknologi MARA, Shah Alam, Selangor, Malaysia
[3]Centre of Chemical Synthesis and Polymer Technology (CCSPT), Institute of Science (IOS), Universiti Teknologi MARA, Shah Alam, Selangor, Malaysia

Abstract. The construction of binary heterostructures is an effective strategy to enhance photocatalytic efficiency. In this study, a type-II TiO_2/g-C_3N_4 heterostructure was synthesized via a solvothermal method, with 0D TiO_2 nanoparticles uniformly dispersed on 2D g-C_3N_4 nanosheets. The optimal TiO_2 to g-C_3N_4 ratio (5:1) achieved superior tetracycline (TC) degradation. Characterization using XRD, FESEM, BET, UV-DRS and EIS revealed improved light absorption, enhanced charge separation and strong interfacial interactions. Electrochemical impedance spectroscopy confirmed suppressed charge recombination and prolonged carrier lifetimes. The heterostructure retained 85.47% of its photocatalytic activity after four cycles, demonstrating excellent stability. Mechanistic studies identified holes (h^+) and superoxide radicals ($\bullet O_2^-$) as key reactive species, confirming a type-II heterojunction that facilitated charge transfer. The results demonstrated the role of g-C_3N_4 in modulating TiO_2 activity, highlighting the potential of TiO_2/g-C_3N_4 heterostructures as efficient, durable photocatalysts for environmental remediation.

Keywords: *Heterojunctions, g-C_3N_4, photocatalytic degradation, tetracycline.*

****Corresponding Author:*** *Lim Ying Chin, School of Chemistry and Environment, Faculty of Applied Sciences, Universiti Teknologi MARA, Shah Alam, Selangor, Malaysia, Tel.:+60355444533; e-mail: limyi613@uitm.edu.my*

Received: *6 April 2025;* ***Accepted:*** *29 May 2025;* ***Published:*** *5 August 2025.*

1. Introduction

Antibiotics have long been indispensable in safeguarding human health and driving the development and growth of the livestock and aquaculture industries. However, their excessive and improper use has resulted in accumulation of significant residues in aquatic ecosystems, primarily through excretion from humans and animals, as well as the discharge of inadequately treated or untreated wastewater (Huang *et al.*, 2022). This widespread contamination poses a serious threat to environmental safety and ecological balance. Among the various classes of antibiotics, tetracycline antibiotics have seen particularly extensive global use resulting in increasing environmental risks. Although these antibiotics effectively eliminate pathogenic microorganisms in the aquatic environments, they inadvertently disrupt the activity of beneficial microbial communities leading to ecological imbalances. Additionally, the persistent presence of even trace amounts of tetracycline over prolonged periods can stimulate the development of antibiotic-resistant bacteria, thereby increasing the threat to human and animal health

(Liao *et al*., 2021; Ni *et al*., 2022). This growing concern requires the urgent need for effective strategies to mitigate the environmental impact of tetracycline residues and to curb the rise of antibiotic resistance.

In response to the escalating environmental risks posed by tetracycline contamination, various wastewater treatment technologies have been explored and developed, among which photocatalytic oxidation has emerged as a promising approach. This approach garners significant attention as it harnesses solar energy to degrade organic pollutants, offering an environmentally friendly solution for complete contaminant removal (Wang *et al*., 2018; Wu *et al*., 2020; Ahmadi *et al*., 2017, Zhang *et al*., 2020). In this context, TiO_2 has been extensively studied and widely used in photocatalysis owing to its non-toxicity, chemical stability, inexpensive and high catalytic activity (Xie *et al*., 2024). Despite these advantages, its photocatalytic performance is restricted to the ultraviolet region due to wide band gap of 3.2 eV, limiting its effective utilization of the visible light spectrum. Additionally, TiO_2 tends to aggregate during photocatalysis reaction, which reduces the accessibility of active sites and hampers overall efficiency. Researchers have explored composite modification strategies to enhance the visible light-driven photocatalytic performance of TiO_2 by coupling or compositing it with suitable materials such as noble metal, non-metal and semiconductor to address these limitations (Basavarajappa *et al*., 2020; Reddy *et al*., 2023; Ni *et al*., 2021; Qiao *et al*., 2019) Among these, planar graphitic carbon nitride (g-C_3N_4), a metal-free semiconductor, has attracted widespread attention due to its remarkable photoelectric properties, appropriate band gap of 2.7 eV and ability to harness visible light efficiently (Song *et al*., 2020). Additionally, morphology, pore structure and thickness of g-C_3N_4 can be easily tailored through various synthesis methods, making it a versatile candidate for composite formation. Integrating TiO_2 with g-C_3N_4 can effectively combine the strong redox capabilities of TiO_2 with the superior visible light absorption of g-C_3N_4, thereby enhancing photocatalytic efficiency. Recent studies have demonstrated the potential of such binary composites (Liu *et al*., 2024; Zhang *et al*., 2022; Li *et al*., 2022; Zhang *et al*., 2023; Liu *et al*., 2019). For example, Bi et al. (2023) prepared g-C_3N_4/TiO_2 heterojunctions via an absorption-calcination process that exhibited prominent photodegradation efficiency of 90.1% tetracycline under simulated-sunlight irradiation within 30 min, while Chang et al. (2014) synthesized a series of TiO_2 hybrids with exfoliated g-C_3N_4 nanosheets through a facile sol-gel method, attaining much higher catalytic activity for degrading rhodamine B dye. These advancements highlight the efficacy of modifying TiO_2 with g-C_3N_4 and the the potential of this composite strategy to overcome the inherent limitations of TiO_2 to perform under visible light irradiation.

It is well-established that the morphology of a catalyst plays a crucial role in determining its photocatalytic performance. Recently, the innovative strategy of hybridizing zero-dimensional (0D) and two-dimensional (2D) materials has continuously demonstrated remarkable improvements in photocatalytic efficiency (Nawaz *et al*., 2021). Notably, Cheng and Dong (2020) synthesized a metal-free composite via modification of 2D polymeric carbon nitride with 0D graphene quantum dots with enhanced photocatalytic activity in dye degradation. Liang et al. (2021) employed a self-assembled organic supramolecular precursor to grow 0D g-C_3N_4 in situ on 2D BiOI. Resulting in a kinetic constant nearly 22 times higher than that of pure g-C_3N_4 during tetracycline e degradation. Such emerging research works have demonstrated the promising potential 0D/2D heterojunction structures in enhancing photocatalytic degradation performance.

In this work, a binary 0D/2D heterostructures comprising titanium dioxide nanoparticles and g-C_3N_4 nanosheets (TiO_2/g-C_3N_4) was successfully synthesized via a facile hydrothermal method. Uniform dispersion of 0D TiO_2 nanoparticles onto 2D g-C_3N_4 nanosheets effectively prevented the aggregation of particle, thereby maximizing the active surface areas. The strong interfacial interaction between TiO_2 and g-C_3N_4 improved the charge transfer and carrier separation efficiency, which contributed to the enhanced photocatalytic performance compared to the individual components. Systematic investigations were conducted to assess the influence of mass ratio of TiO_2 and g-C_3N_4 on the structural and photoelectrochemical properties of TiO_2/g-C_3N_4 composite. The synthesized composite was extensively characterized through various analytical techniques, confirming its exceptional chemical stability, as further validated by cycling stability tests. Additionally, the underlying mechanism of tetracycline degradation was elucidated using trapping experiments, revealing the roles of reactive species and the pathways involved in the photocatalytic process. These findings highlight the significant potential of 0D/2D heterostructured catalysts for efficient environmental remediation, offering valuable insights into the design of advanced materials for pollutant degradation.

2. Materials and Methods

2.1. Materials

Urea (99.5%) was purchased from Systerm, Malaysia. Titanium dioxide powder was procured from Sigma Aldrich and tetracycline from MedChem Express, USA. Absolute ethanol (99.7%) was purchased from Chemiz, Malaysia. All reagents used are analytical grade and have not undergone further purification. Deionized water was used for all the experimental procedures.

2.2. Preparation of g-C_3N_4

The g-C_3N_4 nanosheets were prepared by a thermal polycondensation process. In this procedure, 20 g urea was carefully placed in a covered crucible and subjected to calcination at 550 ℃ for 3 h with a ramping rate of 180 ℃/h in a muffle furnace. After that, the resulting pale-yellow product underwent a thorough purification process to remove any residual impurities. The g-C_3N_4 powder was washed 10 times with deionised water using a centrifuge before being dried in an oven for 20 hours at 70℃.

2.3. Preparation of TiO_2/g-C_3N_4 (TCN)

TiO_2/g-C_3N_4 composite was synthesized using a facile hydrothermal method, enabling the uniform deposition of zero-dimensional (0D) TiO_2 nanoparticles onto two-dimensional (2D) g-C_3N_4. Initially, 40 mg g-C_3N_4 and 200 mg TiO_2 were ground and mixed thoroughly and placed in a beaker composed of 40 mL deionized water and 20 mL absolute ethanol. Ultrasonication was performed until a homogeneous suspension was achieved. Then prepared dispersion was subsequently transferred into a Teflon-lined stainless-steel autoclave and subjected to hydrothermal treatment at 180 ℃ for 15 h. Following the reaction, the autoclave was allowed to cool naturally to room temperature. The resultant solid was collected and sequentially washed three times with ethanol and deionized water to eliminate any residual impurities. The purified product was then dried in an oven at 60 ℃ for 12 hours to obtain the final TiO_2/g-C_3N_4 composite. The composite

with a TiO_2 to g-C_3N_4 mass ratio of 5:1 was designated as 5:1 TCN. For comparative studies, composites with mass ratios of 10:1 (10:1 TCN) and 30:1 (30:1 TCN) were synthesized under identical conditions, as illustrated in Figure 1.

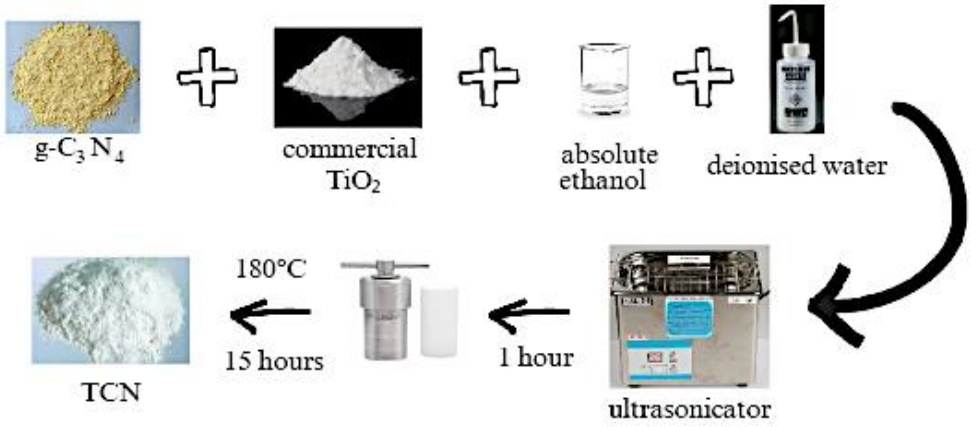

Figure 1. Schematic illustration of the hydrothermal synthesis of TCN composites

2.4. Characterization

The crystalline structures of photocatalysts were analysed by X-ray diffraction (XRD, PANalytical X'pert Pro). The surface morphology of the prepared samples was determined by FESEM (Thermo scientific apreo 2s) and transmission electron microscope (TEM, FEI Tecnai F20). The light absorption of photocatalysts was tested by UV-vis DRS (Agilent, Cary 5000). BET (Micromeritics ASAP 2060) was used to analyse the surface area and pore size distribution of materials. Electrochemical measurements were performed on an Autolab electrochemical workstation (Metrohm Autolab PGSTAT302N) using a standard three-electrode cell with a working electrode, a platinum plate as the counter electrode and a standard Ag/AgCl in saturated KCl as reference electrode. For the working electrodes, 10 mg of photocatalysts were suspended in 5 mL ethanol and the mixtures were ultrasonically dispersed for 30 minutes to form a homogeneous solution. Then, 0.1 mL solution was dropped onto a 1 cm x 1 cm fluorine-tin oxide (FTO) glass electrode with a sheet resistance of 8 Ω and dried using a hotplate. The electrochemical impedance spectroscopies (EIS) were carried out at the open circuit potential in a 0.5 M Na_2SO_4 solution. The amplitude of the sinusoidal wave was 10 mV and the frequency ranged from 10 kHz to 0.01 Hz.

2.5. Photocatalytic Degradation of Tetracycline

Photocatalytic degradation of TC was carried out using a 350 W Xenon lamp to simulate sunlight. Initially, 40 mg TCN composite was introduced into a 100 mL 10 ppm TC solution, obtaining a TCN suspension with a concentration of 0.4 g/L. The mixed liquid underwent a 60-minute stirring in the dark to establish adsorption-desorption equilibrium. Subsequently, the solution was illuminated under simulated sunlight for 3 h and 2 mL suspension was taken out at 30-minute intervals. After being filtered with a 0.22 μm microfiltration membrane, the real-time TC concentration was assessed using a UV–vis spectrophotometer at a characteristic wavelength of 357 nm. The removal efficiency is calculated by the following formula:

$$Removal\ Percentage\ (\%) = 1 - C_t/C_0 \times 100\% \quad (1)$$

where C_t and C_0 are the concentration (mg/L) of TC at time t and initial time.

2.6. Scavengers Test

The active species in the photodegradation of TC solution were determined by radical scavenger experiment. 1 mmol/L ascorbic acid (AA) as a trap for superoxide radicals ($\bullet O_2^-$), EDTA-2Na was used as a scavenger for holes (h^+) and isopropanol (IPA) as a scavenger for hydroxyl radicals (•OH) were used in this study. Apart from adding different scavengers, all other operations remained the same as in the previous experimental procedure.

2.7. Recyclability Study

A recyclability study was carried out to determine the stability of the 5:1 TCN photocatalyst in eliminating TC during several cycles of use. Each photocatalytic treatment was performed using freshly prepared TC solutions. After treatment, 5:1 TCN photocatalyst was filtered, washed several times with deionized water and oven-dried at 70°C overnight to remove the residual TC.

3. Results and Discussion

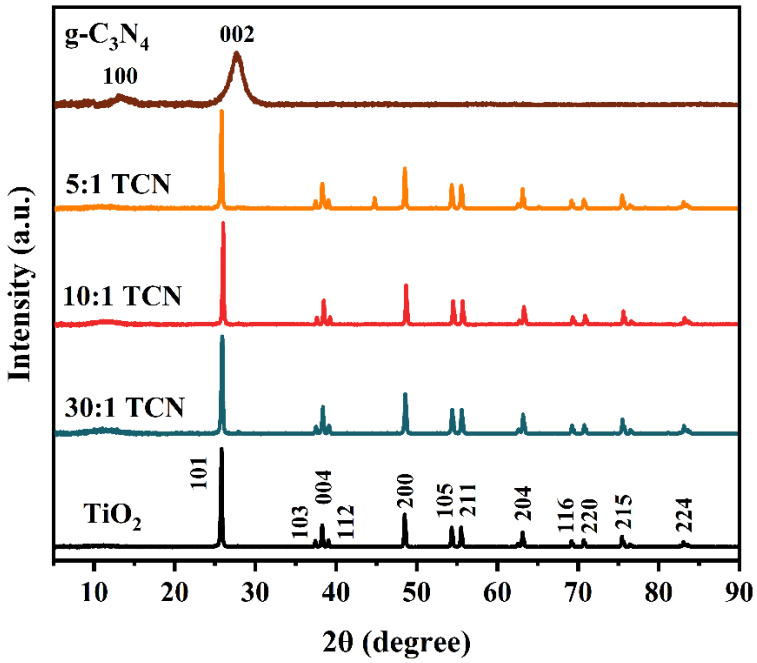

Figure 2. XRD patterns for TiO_2, g-C_3N_4 and TCN composites with different mass ratios

The XRD patterns of TiO_2, g-C_3N_4 and TCN with varying mass ratio (5:1, 10:1 and 30:1 TCN) are shown in Figure 2. The diffraction peaks of TiO_2 exhibited the characteristic of highly crystalline anatase at 2θ = 25.82°, 37.43°, 38.29°, 39.04°, 48.49°, 54.36°, 55.52°, 63.13°, 69.20°, 70.71°, 75.44° and 83.06°conformity to the (101), (103), (004), (112), (200), (105), (211), (204), (116), (220), (215) and (224) crystal planes while

the XRD pattern of g-C_3N_4 exhibited two distinct peaks at 2θ = 13.10° and 27.50°. The weaker diffraction peak at 13.10° corresponds to the (100) plane, which is associated with the interlayer stacking arrangement of aromatic structures. In contrast, the more prominent peak observed at 27.50° is attributed to the (002) crystallographic plane, representing the periodic in-plane structural repetition of tris-s-triazine units within the g-C_3N_4 framework (Li *et al.*, 2025; Wang *et al.*, 2020). This indicates the successful conversion of tris-s-triazine to g-C_3N_4 upon calcination. All the peaks in the 5:1, 10:1 and 30:1TCN spectra were characteristic peaks of TiO_2, however, g-C_3N_4 peak at 13.10° and 27.50° were not detected, which can be attributed to the low loading of g-C_3N_4 in the composites.

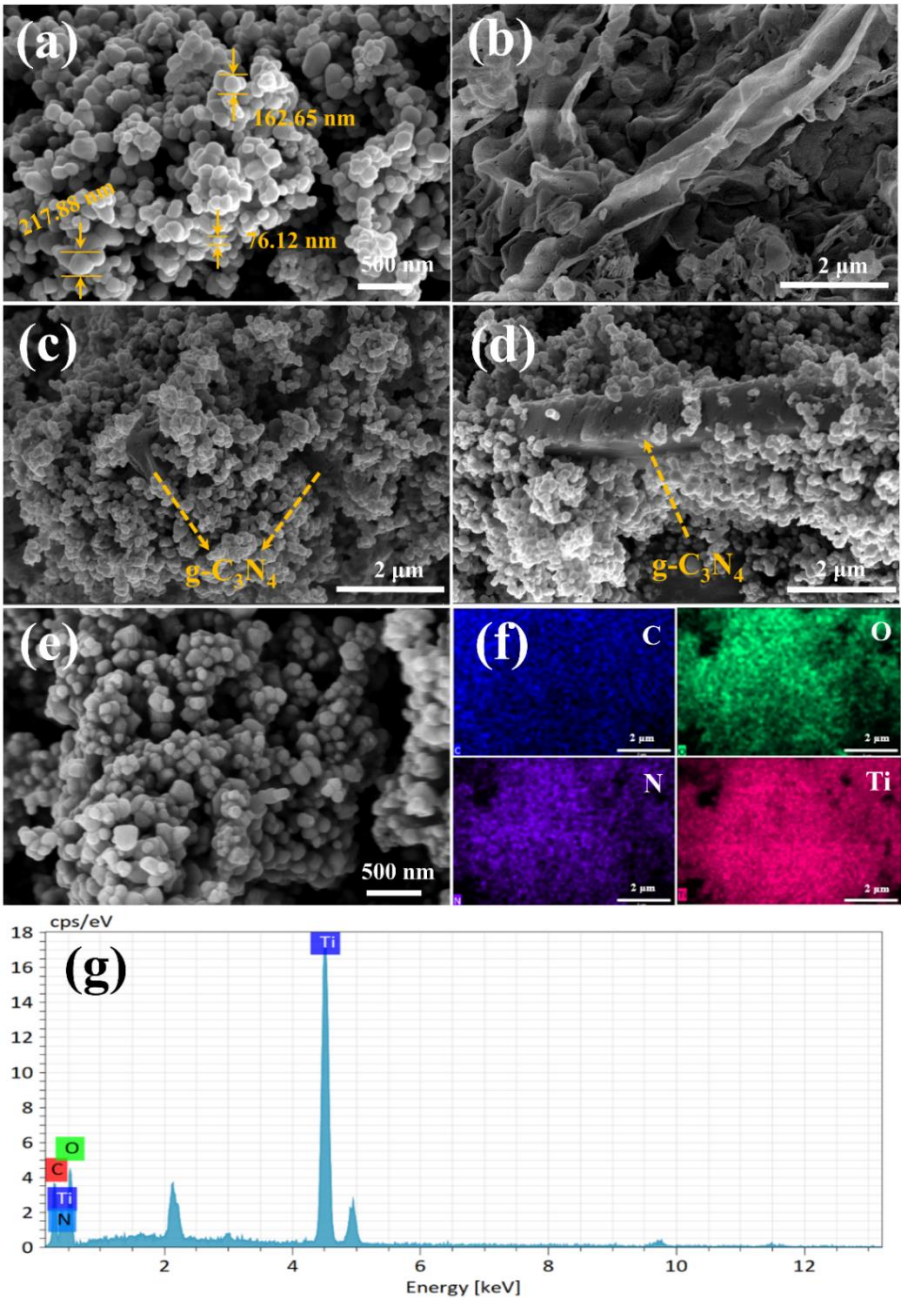

Figure 3. SEM images of (a) TiO_2 (b) g-C_3N_4 (c) 5:1 TCN (d) 10:1 TCN (e) 30:1 TCN (f) EDX mapping (g) spectrum of 5:1 TCN

The FESEM images of TiO_2, g-C_3N_4 and the synthesized TCN composites with varying mass ratio are presented in Figure 3, along with the corresponding elemental map of 5:1 TCN. As illustrated in Figure 2a, the pure TiO_2 exhibits a circular-shaped morphology with particles diameters ranging from 76.12 nm to 217.88 nm. Meanwhile, g-C_3N_4 exhibits an ultrathin sheet-like structure with irregular bending (Figure 2b), which provides an ideal platform for anchoring nanoparticles. This observation is consistent with the previous study reported by Chen et al. (2019). Upon successful formation of 5:1 TCN composite as depicted in Figure 3c, TiO_2 particles are observed to be uniformly distributed and firmly embedded on the surface of g-C_3N_4, confirming the successful integration of the two materials. Furthermore, the EDX mapping and spectral analysis of 5:1 TCN, depicted in Figure 3f and 3g, reveal the presence of distinct signals corresponding to carbon (C), oxygen (O), nitrogen (N) and titanium (Ti), further validating the homogeneous dispersion of TiO_2 particles across the 2D g-C_3N_4 nanosheets. A similar structural configuration is evident in the 10:1 TCN composite (Figure 3d), where TiO_2 particles remain strongly adhered to the g-C_3N_4 surface. However, as the TiO_2 content increases in the 30:1 TCN composite (Figure 3e), the g-C_3N_4 nanosheets become nearly indiscernible, as they are almost entirely covered by an extensive layer of TiO_2 particles.

Further characterization was conducted using Transmission Electron Microscopy (TEM) to accurately elucidate the composite structure. As revealed in the TEM images in Figure 4, the 0D TiO_2 nanoparticles were uniformly anchored onto the surfaces of the 2D g-C_3N_4 nanosheets. The dark regions observed in Figure 4 were attributed to TiO_2, exhibiting distinct lattice fringes with an interplanar spacing of 0.354 nm, corresponding to the (101) crystal plane of anatase TiO_2, which aligns well with the results of the X-ray diffraction (XRD) analysis (Figure 2). In contrast, the light regions were associated with g-C_3N_4, where no lattice fringes were discernible. Notably, a well-defined interface was observed at the contact region, further corroborating the formation of a 0D/2D heterojunction between the TiO_2 nanoparticles and g-C_3N_4 nanosheets.

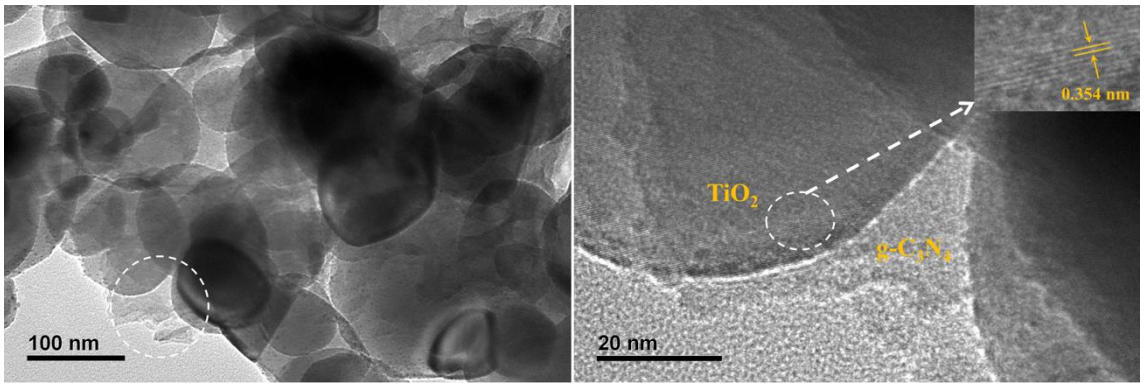

Figure 4. High resolution TEM image of 5:1 TCN composite

BET analysis was employed to evaluate the surface area and porosity of the prepared samples. As can be seen from Figure 5, the nitrogen adsorption-desorption isotherms of TiO_2, g-C_3N_4 and TCN composites exhibit typical IV curves with H3 hysteresis loops, indicating the presence of mesoporous structures. This mesoporous feature is believed to play a crucial role in facilitating molecular diffusion and enhancing photocatalytic activity. The specific surface area values, as summarized in Table 1, reveal

that the composite materials exhibit a reduced surface area compared to their individual counterparts, TiO_2 and g-C_3N_4. Notably, the 5:1 TCN composite demonstrates the lowest specific surface area, measuring 0.96 m^2/g. In conventional photocatalytic systems, an increased specific surface area is generally associated with a higher density of exposed active sites, which enhances photocatalytic efficiency. However, in this study, an inverse trend is observed, where a lower surface area does not necessarily correlate with reduced photocatalytic activity. This finding suggests that the specific surface area is not the predominant factor governing the catalytic performance of the synthesized composites. Instead, other parameters, such as the heterojunction formation between TiO_2 and g-C_3N_4, efficient charge transfer and optimized electronic interactions, may play a more significant role in enhancing the overall photocatalytic efficiency.

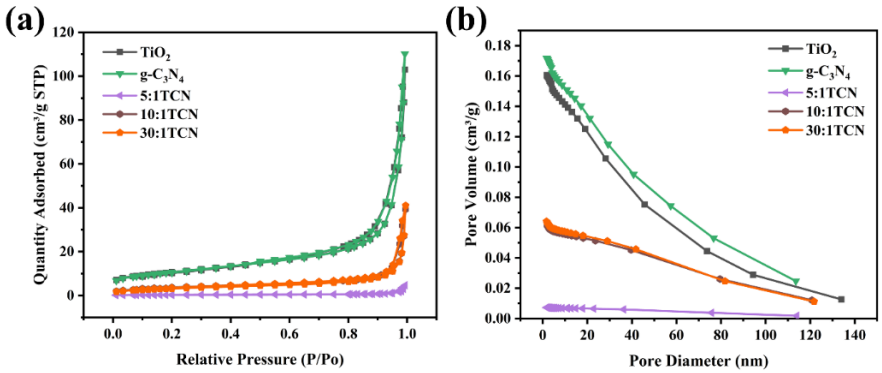

Figure 5. (a) The N_2 adsorption-desorption isotherms samples and (b) corresponding pore size distribution curves of samples

Table 1. Surface area, Pore size and V_{total} of TiO_2, g-C_3N_4 and TCN composites

Composites	Surface area (m^2/g)	Pore size (nm)	V_{total}(cm^3/g)
TiO_2	37.87	18.87	0.1233
g-C_3N_4	37.91	19.73	0.1301
5:1 TCN	0.96	26.39	0.0043
10:1 TCN	12.76	21.36	0.0367
30:1 TCN	11.87	19.68	0.0354

UV-Vis diffuse reflectance spectroscopy (UV-Vis DRS) was employed to evaluate the optical absorption properties of TiO_2, g-C_3N_4 and TCN composites with varying mass ratios. As shown in Figure 6, the absorption spectrum of TiO_2 is predominantly confined to the ultraviolet region with the absorption edge of 390 nm, whereas g-C_3N_4 exhibits broader absorption extending into the visible light region with the absorption shifting to 450 nm. All synthesized TCN composites demonstrated enhanced visible-light absorption capability, with the 5:1 TCN composite showing the most significant improvement, suggesting its potential for application in visible-light-driven photocatalysis. To further elucidate the optical band structure, the bandgap energies of the individual materials were calculated using Tauc plots, based on Kubelka-Munk formula: $(\alpha h\nu)1/n= A(h\nu - Eg)$,

where α, h, ν, n, A and Eg are the absorbance index, Planck's constant, incident photon frequency, semiconductor type, proportionality constant and semiconductor band gap, respectively. The Tauc plot analysis shown in Figure revealed that the band gap values of pristine of TiO_2 and g-C_3N_4 were 3.34 eV and 2.89 eV, respectively, which align well with reported values in the literature (Batoo *et al*., 2024).

Interestingly, the estimated bandgap energy of all TCN composites remained within the range of 3.2-3.25 eV, slightly narrower compared to pristine TiO_2. This observation suggests that the introduction of g-C_3N_4 does not alter the intrinsic electronic structure of composites but rather facilitates improved charge separation and enhanced light absorption. While g-C_3N_4 inherently possesses a narrower bandgap (~2.9 eV), its interaction with TiO_2 in the heterojunction modifies the charge transfer dynamics, thereby is expected to enhance the photocatalytic performance. The enhancement in photocatalytic activity of the composites, despite the minimal bandgap variation, highlights the crucial role of interfacial charge transfer mechanisms in increasing photocatalytic efficiency beyond mere bandgap narrowing.

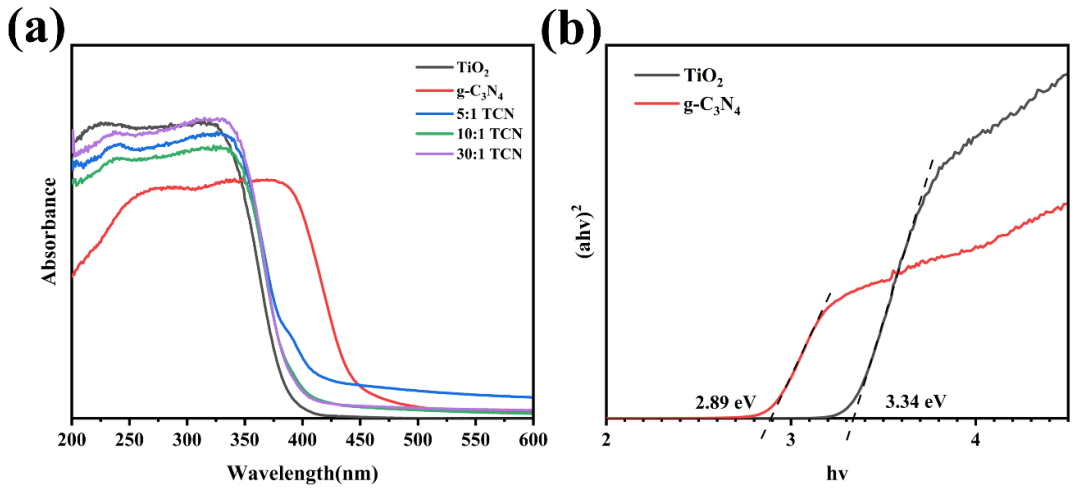

Figure 6. DRS spectra of (a) prepared samples and (b) the plot of $(\alpha h\nu)^2$ vs. hv of pure TiO_2 and g-C_3N_4

Electrochemical Impedance Spectroscopy (EIS) was employed to comprehensively assess the separation and transport properties of photoinduced carriers in the fabricated samples. As shown in Figure 7, the 5:1 TCN composite displays a significantly smaller arc radius compared to both pristine TiO_2 and g-C_3N_4. The reduced arc radius within the impedance spectra indicates a lower charge transfer resistance, signifying enhanced carrier mobility and improved electrical conductivity within the composite (Li *et al*., 2025). This improvement can be attributed to the synergistic integration of TiO_2 and g-C_3N_4, which optimizes charge transport in several ways. Firstly, the intimate interfacial interaction between TiO_2 nanoparticles and g-C_3N_4 sheets facilitates efficient charge transfer pathways, thereby minimizing electron-hole recombination. Additionally, the presence of TiO_2 serves as an effective charge trap, promoting spatial separation of electron-hole pairs and prolonging their lifetimes. Furthermore, the unique structural characteristics of the 5:1TCN composite, as evidenced by SEM analyses, contribute significantly to improved carrier dynamics.

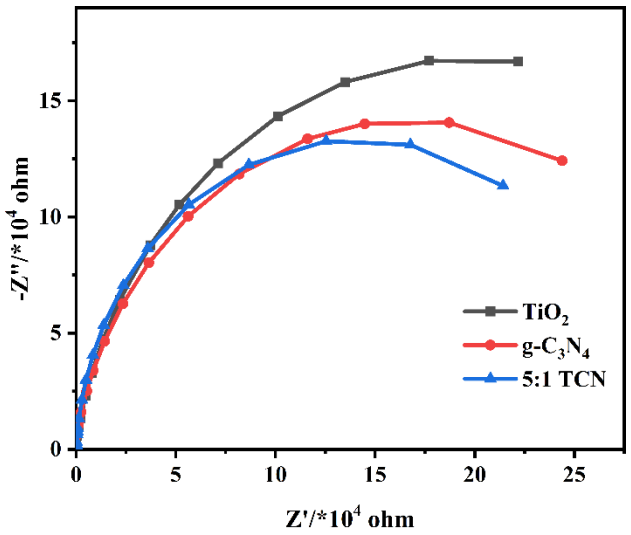

Figure 7. The electrochemical impedance spectra of pure TiO_2, g-C_3N_4 and 5:1TCN samples

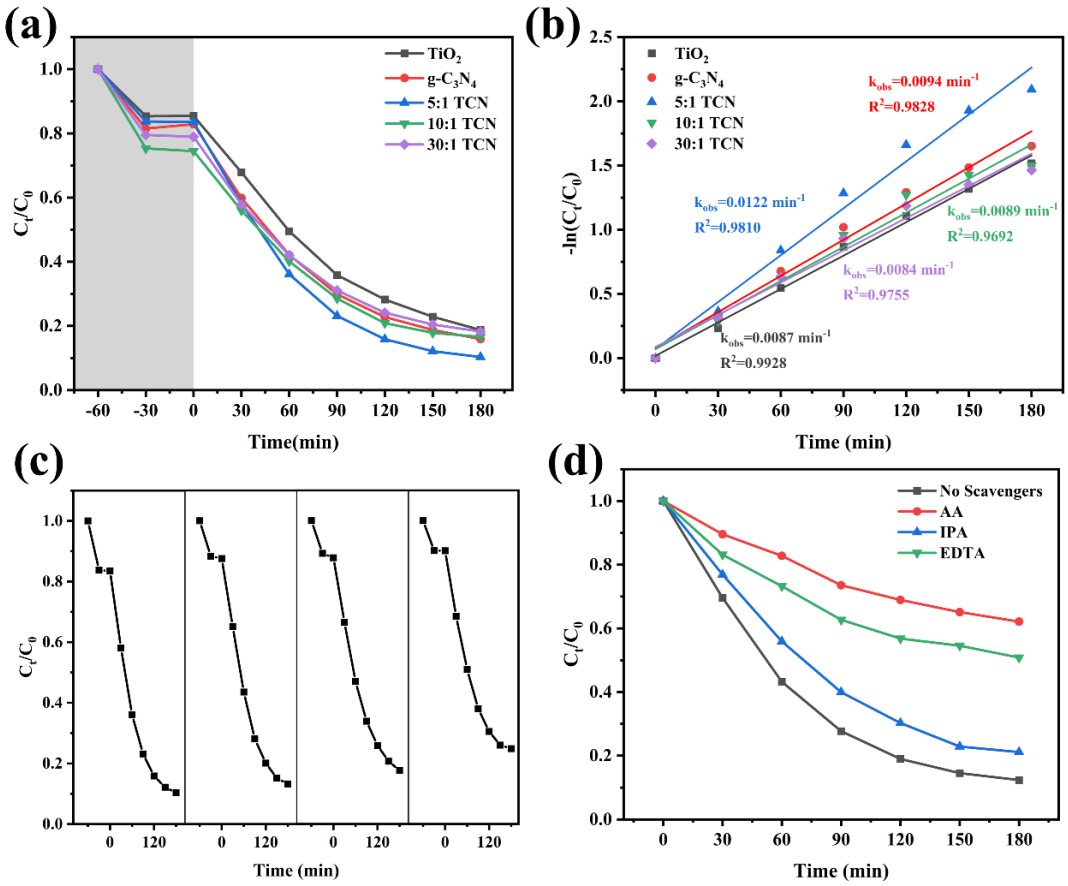

Figure 8. (a) Removal efficiency of TC (b) First-order kinetic model for degradation of TC (c) The cyclic degradation of TC by 5:1 TCN and (d) Scavenger test

The photocatalytic performance of the prepared TCN composites was evaluated by degrading TC using a 350W xenon lamp to simulate visible light. As shown in Figure 8a, after a 60-minute dark reaction, the adsorption-desorption equilibrium was established for all samples. Among the synthesized composites, it is evident that 5:1 TCN composite

has the highest TC removal efficiency, reaching 89.68%, which surpasses that of pure TiO_2 (81.25%) and g-C_3N_4 (84.11%). This enhanced performance is primarily attributed to the synergistic interaction between TiO_2 and g-C_3N_4, which enhances the efficient charge separation and transfer while simultaneously suppressing the recombination of photogenerated electron-hole pairs. However, as the proportion of TiO_2 in the composite increases, the particle aggregation effect become more pronounced, limiting the exposure of active sites and consequently hindering further improvement in the photocatalytic performance.

The photocatalytic degradation kinetics of TC were analysed using a pseudo-first-order kinetic model, described by the equation $-\ln(C_t/C_0) = kt$, where C_0 and C_t are the TC concentration before light radiation and at the radiation time t, respectively and k is the rate constant. As shown in Figure 8b, the k value for the 5:1 TCN composite is significantly higher than that of pure TiO_2 and g-C_3N_4, further confirming its enhanced photocatalytic activity. In addition, cyclic degradation experiments were conducted to evaluate the chemical stability and reusability of the prepared photocatalysts. Following each degradation cycle, the samples were thoroughly washed with deionized water to remove any residual TC. As shown in Figure 8c, after four consecutive cycles, the removal efficiency for TC remained at 75.15%, demonstrating excellent chemical stability and reusability of the 5:1 TCN composite.

Additionally, scavenger experiments were conducted to identify the dominant reactive species involved in the photocatalytic degradation process. AA, IPA and EDTA-2Na were used as scavengers for $\bullet O_2^-$, •OH and h^+ respectively. As illustrated in Figure 8d, the photocatalytic removal efficiency of TC was significantly supressed with the addition of scavengers AA and EDTA-2Na compared to control test, indicating that $\bullet O_2^-$ and h^+ are the main active species playing a decisive role in the photocatalytic degradation process. In contrast, the presence of IPA had a negligible impact on the removal efficiency, suggesting that •OH plays a minimal role in the photocatalytic reaction.

The transport pathways of electrons and holes were investigated to elucidate the photocatalytic mechanism of the as-prepared composite materials. From the Tauc plot results shown in Figure 6b, the conduction band (CB) and valence band (VB) potentials of TiO_2 and g-C_3N_4 were determined using the following equations (Sim *et al*., 2020).

$$E_{CB} = E_{VB} - E_g \quad (2)$$

$$E_{VB} = \chi - E^e + 0.5E_g \quad (3)$$

where χ, E^e, E_g were the geometric average of electronegativity of the composites (5.81 eV for TiO_2, 4.73 eV for g-C_3N_4), free electron energy (4.5 eV vs. NHE) and band gap (3.34 eV for TiO_2, 2.89 eV for g-C_3N_4), respectively. The calculated CB and VB potentials of TiO_2 are -0.37 eV and 2.97 eV, respectively, while those of g-C_3N_4 are -1.215 eV and 1.675 eV. Consequently, a proposed mechanism for the charge separation and transport at the heterojunction interface is illustrated in Figure 9. Trapping experiments have demonstrated that hydroxyl radicals (•OH) are not the primary reactive species in the photocatalytic process. This observation suggests that photogenerated holes (h^+) in the VB of TiO_2 transfers to the more negative VB of g-C_3N_4, thereby suppressing the generation of sufficient •OH radicals. Instead, the h^+ species in g-C_3N_4 play a direct role in the oxidative degradation of TC. Additionally, the CB potential of g-C_3N_4 is more negative than that of TiO_2, facilitating the efficient transfer of photogenerated electrons

from the CB of g-C_3N_4 to the CB of TiO_2 through the tight heterojunction interface. Furthermore, the CB edge potential of TiO_2 is sufficiently more negative relative to the standard redox potential of $O_2/•O_2^-$, allowing the accumulated electrons in the CB of TiO_2 to react with adsorbed O_2 molecules (Hou *et al.*, 2022). This reaction leads to the formation of sufficient amount of superoxide radicals ($•O_2^-$), which contribute to the oxidative degradation of TC, aligning well with the trapping experiment results. Thus, the electron and hole transport pathways in the 5:1 TCN composite conform to a type-II heterojunction mechanism. This configuration effectively suppresses the recombination of photogenerated charge carriers, thereby significantly enhancing the photocatalytic efficiency of TC degradation.

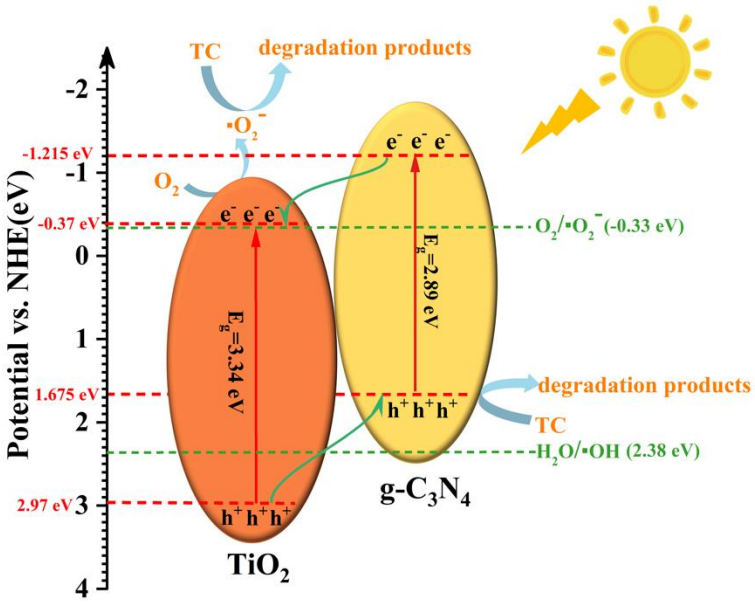

Figure 9. The proposed photocatalytic mechanism for the degradation of TC on the surface of 5:1 TCN composites

4. Conclusion

In this study, type-II 0D/2D TiO_2/g-C_3N_4 heterostructure photocatalysts with the distinct mass ratio of TiO_2 to g-C_3N_4 were successfully fabricated via facile solvothermal reaction and applied for TC degradation. The photocatalytic degradation efficiency for TC was effectively enhanced by 5:1 TCN composite under simulated sunlight irradiation, reaching 89.68%, as evidenced by the PFO kinetic model. Enhanced separation and transport ability of photogenerated electron-hole pairs was demonstrated in electrochemical performance tests, attributed to the formation of a tight heterostructure with 0D TiO_2 particles anchored on 2D g-C_3N_4 nanosheets, effectively suppressing electron-hole recombination. With h^+ and $•O_2^-$ identified as the primary active species and the appropriate matching of CB and VB between TiO_2 and g-C_3N_4, the type-II heterojunction mechanism was confirmed. Additionally, the removal efficiency for TC remaining at 75.15% after four photocatalytic cycles indicated that 5:1 TCN retains excellent reusability and chemical stability. This study emphasizes the regulatory role of g-C_3N_4 in the construction of type-II heterojunctions to improve photocatalytic performance.

Acknowledgments

This study was financially supported by Universiti Teknologi MARA under the GPM Research Grant (600-RMC 5/3/GPM (084/2023).

References

Ahmadi, M., Motlagh, H.R., Jaafarzadeh, N., Mostoufi, A., Saeedi, R., Barzegar, G. & Jorfi, S. (2017). Enhanced photocatalytic degradation of tetracycline and real pharmaceutical wastewate using MWCNT/TiO_2 nano-composite. *Journal of Environmental Management*, 186, 55-63.

Basavarajappa, P.S., Patil, S.B., Ganganagappa, N., Reddy, K.R., Raghu, A.V. & Reddy, C.V. (2020). Recent progress in metal-doped TiO_2, non-metal doped/codoped TiO_2 and TiO_2 nanostructured hybrids for enhanced photocatalysis. *International Journal of Hydrogen Energy*, *45*(13), 7764-7778.

Batoo, K.M., Jassim, K.H., Qassem, T.A., Hussain, S., Hasson, W.T., Jalal, S.S., … & Alsaalamy, A. (2024). Novel magnetically separable g-C_3N_4/TiO_2/$CuFe_2O_4$ photocatalyst for efficient degradation of tetracycline under visible light irradiation: Optimization of process by RSM. *Journal of Saudi Chemical Society*, *28*(3), 101871.

Bi, R., Liu, J., Zhou, C., Shen, Y., Liu, Z. & Wang, Z. (2023). In situ synthesis of g-C_3N_4/TiO_2 heterojunction by a concentrated absorption process for efficient photocatalytic degradation of tetracycline hydrochloride. *Environmental Science and Pollution Research*, *30*(19), 55044-55056.

Chang, F., Zhang, J., Xie, Y., Chen, J., Li, C., Wang, J., ... & Hu, X. (2014). Fabrication, characterization and photocatalytic performance of exfoliated g-C_3N_4–TiO_2 hybrids. *Applied Surface Science*, 311, 574-581.

Chen, X., Shi, R., Chen, Q., Zhang, Z., Jiang, W., Zhu, Y. & Zhang, T. (2019). Three-dimensional porous g-C_3N_4 for highly efficient photocatalytic overall water splitting. *Nano Energy*, 59, 644-650.

Cheng, L., Dong, X. (2020). Carbonaceous 0D/2D composite photocatalyst for degradation of organic dyes. *Diamond and Related Materials*, 109, 108096.

Hou, L., Li, W., Wu, Z., Wei, Q., Yang, H., Jiang, Y., ... & He, Q. (2022). Embedding ZnCdS@ $ZnIn_2S_4$ into thiazole-modified g-C_3N_4 by electrostatic self-assembly to build dual Z-scheme heterojunction with spatially separated active centers for photocatalytic H2 evolution and ofloxacin degradation. *Separation and Purification Technology*, 290, 120858.

Huang, F., Chen, L., Zhang, C., Liu, F. & Li, H. (2022). Prioritization of antibiotic contaminants in China based on decennial national screening data and their persistence, bioaccumulation and toxicity. *Science of the Total Environment*, 806, 150636.

Li, Q., Wang, Z., Li, Y. & Zhang, H. (2025). Degradation of tetracycline hydrochloride through g-C_3N_4/TiO_2 nanotube arrays for photoelectrocatalytic activation of PMS system: Performance and mechanistic analysis. *Materials Science in Semiconductor Processing*, 185, 108879.

Li, Y., Zhang, Q., Lu, Y., Song, Z., Wang, C., Li, D., ... & Zhou, X. (2022). Surface hydroxylation of TiO_2/g-C_3N_4 photocatalyst for photo-Fenton degradation of tetracycline. *Ceramics International*, *48*(1), 1306-1313.

Liang, J., Li, X., Zuo, J., Lin, J. & Liu, Z. (2021). Hybrid 0D/2D heterostructures: in-situ growth of 0D g-C_3N_4 on 2D BiOI for efficient photocatalyst. *Advanced Composites and Hybrid Materials*, 4, 1122-1136.

Liao, Q., Rong, H., Zhao, M., Luo, H., Chu, Z. & Wang, R. (2021). Interaction between tetracycline and microorganisms during wastewater treatment: A review. *Science of the Total Environment*, 757, 143981.

Liu, C., Dong, S. & Chen, Y. (2019). Enhancement of visible-light-driven photocatalytic activity of carbon plane/g-C_3N_4/TiO_2 nanocomposite by improving heterojunction contact. *Chemical Engineering Journal*, 371, 706-718.

Liu, R., Zhang, X., Han, X., Sun, Y., Jin, S. & Liu, R. J. (2024). Photocatalytic degradation of tetracycline with Fe_3O_4/g-C_3N_4/TiO_2 catalyst under visible light. *Carbon Letters*, *34*(1), 75-83.

Nawaz, A., Goudarzi, S., Asghari, M.A., Pichiah, S., Selopal, G.S., Rosei, F., ... & Zarrin, H. (2021). Review of hybrid 1D/2D photocatalysts for light-harvesting applications. *ACS Applied Nano Materials*, *4*(11), 11323-11352.

Ni, J., Wang, W., Liu, D., Zhu, Q., Jia, J., Tian, J., ... & Xing, Z. (2021). Oxygen vacancy-mediated sandwich-structural TiO_2−x/ultrathin g-C_3N_4/TiO_2−x direct Z-scheme heterojunction visible-light-driven photocatalyst for efficient removal of high toxic tetracycline antibiotics. *Journal of Hazardous Materials*, 408, 124432.

Ni, S., Fu, Z., Li, L., Ma, M. & Liu, Y. (2022). Step-scheme heterojunction g-C_3N_4/TiO_2 for efficient photocatalytic degradation of tetracycline hydrochloride under UV light. *Colloids and Surfaces A: Physicochemical and Engineering Aspects*, 649, 129475.

Qiao, H., Huang, Z., Liu, S., Tao, Y., Zhou, H., Li, M. & Qi, X. (2019). Novel mixed-dimensional photocatalysts based on 3D graphene aerogel embedded with TiO_2/MoS_2 hybrid. *The Journal of Physical Chemistry C*, *123*(17), 10949-10955.

Reddy, N.R., Reddy, P.M., Jyothi, N., Kumar, A.S., Jung, J.H. & Joo, S.W. (2023). Versatile TiO_2 bandgap modification with metal, non-metal, noble metal, carbon material and semiconductor for the photoelectrochemical water splitting and photocatalytic dye degradation performance. *Journal of Alloys and Compounds*, 935, 167713.

Sim, L.C., Koh, K.S., Leong, K.H., Chin, Y.H., Abd Aziz, A. & Saravanan, P. (2020). In situ growth of g-C_3N_4 on TiO_2 nanotube arrays: Construction of heterostructures for improved photocatalysis properties. *Journal of Environmental Chemical Engineering*, *8*(1), 103611.

Song, J., Wu, X., Zhang, M., Liu, C., Yu, J., Sun, G., Si, Y. & Ding, B. (2020). Highly flexible, core-shell heterostructured and visible-light-driven titania-based nanofibrous membranes for antibiotic removal and E. coil inactivation. *Chemical Engineering Journal*, 379, 122269.

Wang, D., Jia, F., Wang, H., Chen, F., Fang, Y., Dong, W., ... & Yuan, X. (2018). Simultaneously efficient adsorption and photocatalytic degradation of tetracycline by Fe-based MOFs. *Journal of Colloid and Interface Science*, 519, 273-284.

Wang, Y., Rao, L., Wang, P., Shi, Z. & Zhang, L. (2020). Photocatalytic activity of N-TiO_2/O-doped N vacancy g-C_3N_4 and the intermediates toxicity evaluation under tetracycline hydrochloride and Cr (VI) coexistence environment. *Applied Catalysis B: Environmental*, 262, 118308.

Wu, S., Hu, H., Lin, Y., Zhang, J. & Hu, Y. H. (2020). Visible light photocatalytic degradation of tetracycline over TiO_2. *Chemical Engineering Journal*, 382, 122842.

Xie, W., Liu, G., Liu, Y., Bai, Y., Liao, Y., Li, T., ... & Hu, J. (2024). Multidimensional TiO_2 photocatalysts for the degradation of organic dyes in wastewater treatment. *Journal of Porous Materials*, *31*(5), 1655-1681.

Zhang, B., He, X., Yu, C., Liu, G., Ma, D., Cui, C., ... & Xin, Y. (2022). Degradation of tetracycline hydrochloride by ultrafine TiO_2 nanoparticles modified g-C_3N_4 heterojunction photocatalyst: Influencing factors, products and mechanism insight. *Chinese Chemical Letters*, *33*(3), 1337-1342.

Zhang, J., Wang, X., Shen, K., Lu, W., Wang, J. & Chen, F. (2023). Defect engineering in g-C_3N_4 quantum-dot-modified TiO_2 nanofiber: Uncovering novel mechanisms for the degradation of tetracycline in coexistence with Cu^{2+}. *Advanced Fiber Materials*, *5*(1), 168-182.

Zhang, Q., Jiang, L., Wang, J., Zhu, Y., Pu, Y. & Dai, W. (2020). Photocatalytic degradation of tetracycline antibiotics using three-dimensional network structure perylene diimide supramolecular organic photocatalyst under visible-light irradiation. *Applied Catalysis B: Environmental*, 277, 119122.